ACS APPLIED MATERIALS & INTERFACES

Research Article

www.acsami.org

Unzipped Multiwalled Carbon Nanotube Oxide/Multiwalled Carbon Nanotube Hybrids for Polymer Reinforcement

Jinchen Fan,[†] Zixing Shi,*[,†] Ming Tian,[‡] Jialiang Wang,[†] and Jie Yin[†]

[†]School of Chemistry and Chemical Technology, State Key Laboratory for Metal Matrix Composite Materials, Shanghai Jiao Tong University, 200240, Shanghai, People's Republic of China

[‡]State Key Laboratory of Organic−Inorganic Composites, Beijing University of Chemical Technology, 100029, Beijing, People's Republic of China

Supporting Information

ABSTRACT: Multiwalled carbon nanotubes (MWNTs) have been widely used as nanofillers for polymer reinforcement. However, it has been restricted by the limited available interface area of MWNTs in the polymer matrices. Oxidation unzipping of MWNTs is an effective way to solve this problem. The unzipped multiwalled carbon nanotube oxides (UMCNOs) exhibit excellent enhancement effect with low weight fractions, but agglomeration of UMCNOs at a relatively higher loading still hampered the mechanical reinforcement of polymer composites. In this paper, we interestingly found that the dispersion of UMCNOs in polymer matrices can be significantly improved with the combination of pristine MWNTs. The hybrids of MWNTs and UMCNOs (U/Ms) can be easily obtained by adding the pristine MWNTs into the UMCNOs aqueous dispersion, followed by sonication. With a π-stacking interaction, the UMCNOs were attached onto the outwalls of MWNTs. The morphologies and structure of the U/Ms were characterized by several measurements. The mechanical testing of the resultant poly(vinyl alcohol) (PVA)-based composites demonstrated that the U/Ms can be used as ideal reinforcing fillers. Compared to PVA, the yield strength and Young's modulus of U/M−PVA composites with a loading of 0.7 wt % of the U/Ms approached ∼145.8 MPa and 6.9 GPa, respectively, which are increases of ∼107.4% and ∼122.5%, respectively. The results of tensile tests demonstrated that the reinforcement effect of U/Ms is superior to the individual UMCNOs and MWNTs, because of the synergistic interaction of UMCNOs and MWNTs.

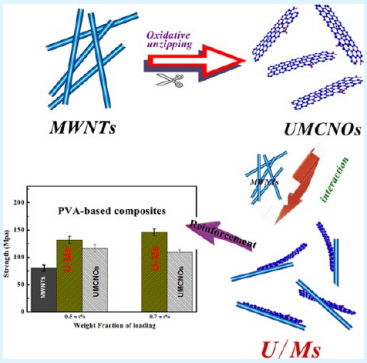

KEYWORDS: *reinforcement, multiwalled carbon nanotube, unzipped multiwalled carbon nanotube oxide*

1. INTRODUCTION

Carbon nanotubes (CNTs) can be viewed as cylinders that consist of seamlessly rolled graphene sheets. Because of their high flexibility, low mass density, and large aspect ratio (typically >1000), CNTs have always been considered as reinforcing fillers for polymer matrixes to achieve high performance and multifunction.[1−5] CNTs can be classified into two major types, namely, single-walled carbon nanotubes (SWNTs) and multiwalled carbon nanotubes (MWNTs), according to the number of the rolled graphene sheets.[6−9] However, the difficult in separating SWNTs from bundles into individual nanotubes is still a big challenge for the use of SWNT in real application. In addition, the high cost and difficulty in purification also limits the large-scale production of SWNTs. In contrast, for CVD-growth MWNTs, the cost is much lower.[10−16] Therefore, MWNTs have been widely used as mechanical reinforcement agents over the past few years.[17−24]

The efficiency of load transfer between the walls of MWNTs and the polymer matrix and the nanofillers is the key factor that governs the strength of the final polymer composites.[25−27] However, the enhancement of mechanical properties of MWNTs-based polymer composites has been greatly hampered by its poor structural reinforcement. There are reasons for this, which include reduced interfacial contact area, since the outermost nanotube shields the internal tubes from the polymer matrix, poor wetting and interfacial adhesion with polymer matrix, and intertube slip within the concentric nanotube cylinders, leading to a "sword-in-sheath type" failure.[28−30] Tour's group first prepared graphene oxide nanoribbons (GONRs) by oxidation unzipping MWNTs.[31] It is demonstrated that graphene nanoribbon (GNR) exhibits outstanding electrical and physical properties, better than those of MWNTs.[32,33] Rafiee and co-workers reported that the GNRs obtained by oxidative unzipping MWNTs are superior to the pristine MWNTs with regard to improving the mechanical properties of epoxy.[34] After unzipping, the UMCNOs can address this intrinsic limitation of MWNTs as reinforced fillers. As a result of the high surface area and ribbon-like geometry, UMCNOs indeed show significant potential in polymer composites as a structural reinforcement additive.[35] However, it is found that UMCNOs are still liable to agglomerate in a

Received: August 11, 2012
Accepted: November 2, 2012
Published: November 2, 2012

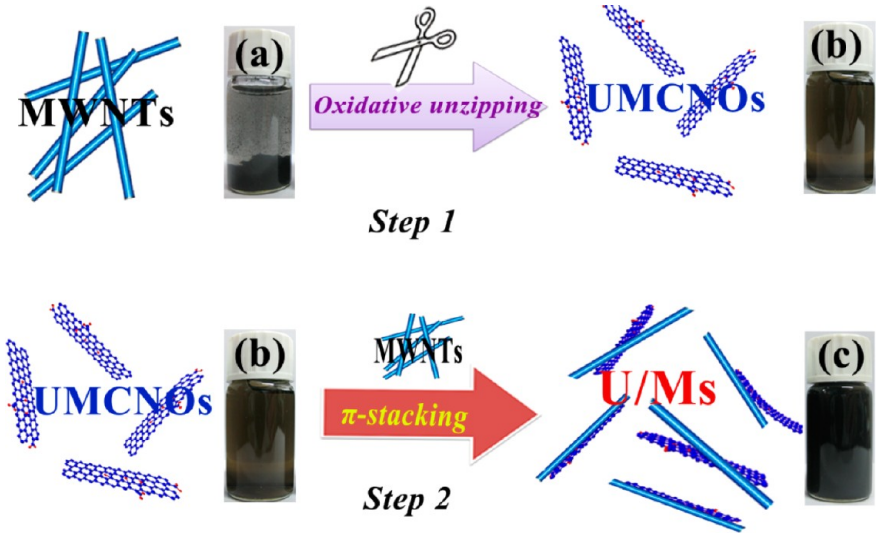

Figure 1. Schematic drawing of preparation steps for the U/Ms and photographs of aqueous dispersions of (a) MWNTs, (b) UMCNOs (0.1 mg/mL), and (c) U/Ms (0.1 mg/mL).

polymer matrix, even at low weight fractions. The tendency of agglomeration with increasing high loading fractions restricts the realization of the full benefit of these unique materials for structural composites.[34,36]

It is well-known that graphene has attracted a great deal of attention in reinforcing nanofillers, because of its large surface areas and excellent physical properties.[37] The efficient reinforcement was also limited by the agglomeration of graphene in the polymer matrix.[38,39] Liu et al. reported a noncovalent method for dispersing and stabilizing the reduced graphene oxide (RGO) with acid-treated MWNTs by $\pi-\pi$ stacking interaction.[40] The obtained reduced graphene oxide/acid-treated MWNT hybrids were demonstrated to be ideal reinforcing nanofillers for polymer composites. Liao et al. studied the incorporation reinforcement effect of GO and MWNTs by directly adding the GO and MWNTs together into the PVA matrix. Because of the synergistic effect, the ternary blends (GO/MWNTs/PVA) can result in an obvious improvement in the yield strength and Young's modulus of PVA.[41]

In fact, the multiple aromatic regions of GO could interact with the outer walls of MWNTs with π-stacking interaction.[42,43] Based on the above consideration, we used the UMCNOs to disperse the pristine MWNTs in aqueous solution. With the assist of π-stacking interaction, the UMCNO/MWNT hybrids (U/Ms) were prepared by directly adding pristine MWNTs to the UMCNO aqueous dispersion, followed by sonication. The as-prepared U/Ms can be well-dispersed in aqueous solution. Therefore, U/Ms could be acted as novel nanofillers for polymer reinforcement. PVA was chosen as a model polymer for studying the enhancing effect of mechanical properties in detail. The results of tensile tests demonstrated that U/Ms were more effective than the individual MWNTs and UMCNOs in polymer reinforcement.

2. EXPERIMENTAL SECTION

2.1. Materials. MWNTs (purity, >95%; length, ~10 μm; diameter, >30 nm) were purchased from Chengdu Organic Chemistry Co., Ltd. (China). Poly(vinyl alcohol) (PVA AH-26; degree of polymerization, ~2600; hydrolysis degree, ~98%) was purchased from Shanghai Chemical Reagents Co., Ltd. (China). Concentrated sulfuric acid (95%–98%), potassium permanganate ($KMnO_4$), hydrogen peroxide (H_2O_2, 30%), and concentrated hydrochloric acid were also received from Sinopharm Chemical Reagent Co., Ltd. (SCRC), and used without any purification.

2.2. Preparation of the UMCNOs. The UMCNOs were produced using the oxidative unzipping method, as first reported by Tour's group.[31] First, 0.2 g of MWNTs was suspended in 100 mL of concentrated sulfuric acid under stirring for 2 h. Then, 1.0 g of $KMnO_4$ was slowly added to the suspension. Successively, the mixture was stirred for 1 h at room temperature and another 1 h at 70 °C. After the reaction, the mixture solution was poured into ice water by adding of 5 mL of a 30 wt % H_2O_2 water solution. The mixture was filtered over a PTFE membrane with a 0.45-μm pore size. The filter cake was centrifuged and extensively washed six times with a 1:10 hydrochloric acid aqueous solution and four times with deionized (DI) water. Finally, the UMCNOs were dried under vacuum at 60 °C for 12 h.

2.3. Preparation of U/Ms. UMCNOs were first dispersed in water (1.0 mg mL^{-1}) by sonication for 1 h and centrifuged at 4000 rpm for 30 min to further remove aggregates. The obtained supernatants were used to disperse MWNTs throughout all of the experiments. Then, the MWNTs were added into the supernatants, followed by sonication for 2 h at room temperature. After the sonication, this suspension was centrifuged at 2000 rpm for 30 min to remove the unstabilized MWNTs, thus giving a dispersion of the U/Ms hybrids and the residual UMCNOs sheets in the supernatant. Next, the U/Ms hybrids were separated from the residual UMCNOs by repeated centrifugation at 8000 rpm for 30 min and water-washing steps. By collecting the sediment, U/Ms were obtained by lyophilizing the sediment in a freeze-dry system for 72 h to remove water completely.

2.4. Fabrication of U/M–PVA Composite Films. A typical procedure for the fabrication of U/M–PVA composite films, the UMCNOs aqueous dispersion was obtained by adding the required amount of U/Ms into 5 mL of water, followed by sonication for 30 min, to yield a homogeneous solution. Meanwhile, 1.0 g of PVA was dissolved in 10 mL of water at 90 °C for 1 h to give a 10 wt % solution. Then, these two solutions were subjected to being mixed together, with 4 h of stirring for effective mixing and 10 min of sonication for the removal of trapped air bubbles. Finally, the homogeneous U/M–PVA mixture solutions were cast onto a circular dish with a diameter of 8 cm under horizontal conditions and flattened to a uniform thickness using a flat blade. The U/M–PVA composite films were dried at 40 °C for 24 h. For completely removing the water, the U/M–PVA composite films were further dried under vacuum at 60 °C for 6 h. By varying the amount of U/Ms, U/M–PVA composite films with different weight fractions of U/Ms were obtained. In addition, MWNT–PVA and UMCNO–PVA composite films were also prepared using a similar procedure, for the sake of comparison.

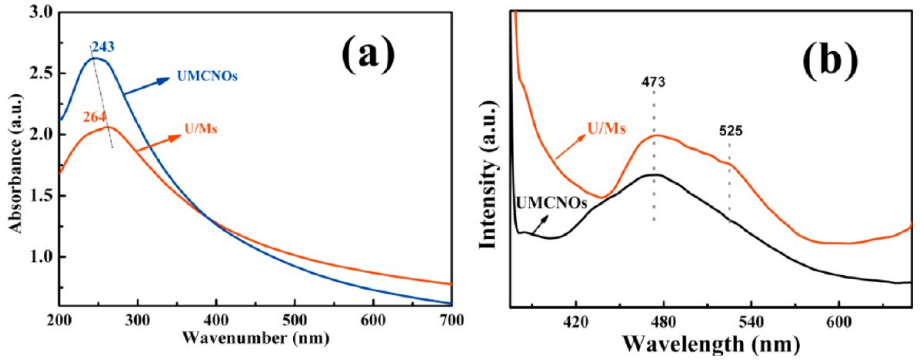

Figure 2. (a) UV–vis absorption spectra of the UMCNOs and U/Ms aqueous dispersions. (b) Emission spectra of the UMCNOs and U/Ms aqueous dispersion (excitation wavelength, λ_{max} = 350 nm).

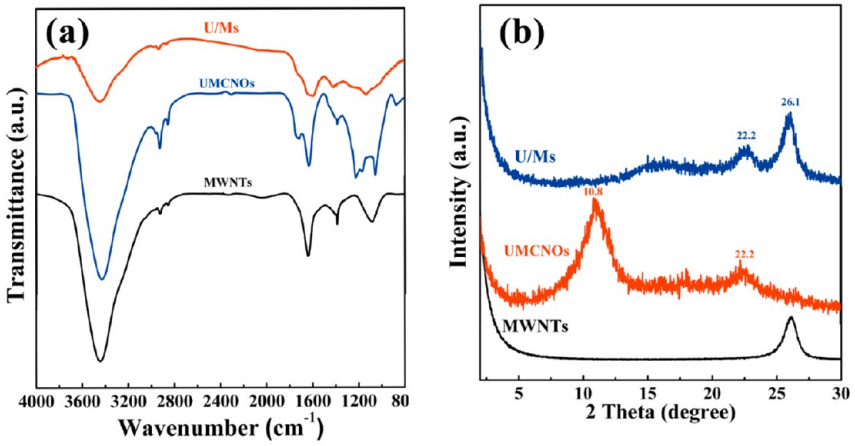

Figure 3. (a) FTIR spectra of pristine MWNTs, UMCNOs, and U/Ms. (b) XRD patterns of the MWNTs, UMCNOs, and U/Ms.

2.5. Characterization and Instruments. Fourier transform infrared (FTIR) spectra were recorded on a Perkin–Elmer Paragon 1000PC spectrometer. Powder X-ray diffraction (XRD) patterns were recorded on a D/max-2200/PC (Japan Rigaku Corp.) using Cu Kα radiation (λ = 1.5418 Å). Raman spectra were taken with a Jobin–Yvon micro-Raman spectroscopy system (Model RamLab-010), equipped with a holographic grating of 1800 lines/mm and a He–Ne laser (632.8 nm) as an excitation source. The emission spectra were recorded on a Perkin–Elmer LS 50B luminescence spectrometer at room temperature. Thermogravimetric analysis (TGA) was performed in nitrogen with a Perkin–Elmer TGA 2050 instrument at a heating rate of 20 °C/min. The tensile properties of the composite films were measured with an Instron 4465 instrument at room temperature with a humidity of ~30% at a crosshead speed of 4 mm/min and an initial gauge length of 40 mm, samples were cut into strips of 60 mm × 4 mm using a razor blade, and five strips were measured for each sample. The fracture surfaces of composite films were characterized by scanning electron microscopy (SEM) (Model JSM-7401F, JEOL). The morphologies of MWNTs and UMCNOs were obtained using transmission electron microscopy (TEM) (Model 2100F, JEOL). Optical microscope images of composite films were obtained using an Olympus Model GX51 microscope. The degree of crystallinity of the samples was measured via differential scanning calorimetry (DSC) (Model 6200, Seiko, Japan). The zeta potential values of the MWNTs, UMCNOs, and U/Ms were measured in aqueous solution at the same pH (4.6), using a Zetasizer 2000 (Malvern Instruments, U.K.).

3. RESULTS AND DISCUSSION

The method of oxidative unzipping of MWNTs was first reported by Tour's group to fabricate GONRs.[31] We have not used the acronym "GONR" to represent the UMCNOs because the obtained UMCNOs were not totally unzipped and exfoliated to the GNR, since the raw MWNTs that we used possessed different crystalline structures and the agglomerations of MWNTs might cause an inhomogeneous reaction with the oxidant (see Figure S2 in the Supporting Information).

3.1. Preparation of U/Ms. As shown in Figure 1a, the pristine MWNTs cannot form a stable dispersion in water, even after a long sonication time. However, UMCNOs possess good dispersibility in water, because of the introduction of hydrophilic groups during the process of oxidative unzipping MWNTs (see Figure 1b). The UMCNO aqueous dispersion used here was the top supernatant with high stability by centrifuging at 4000 rpm for 30 min. For preparing U/Ms, the pristine MWNTs were added into the UMCNOs aqueous dispersion with 2 h of sonication. After sonication, the brown-yellow UMCNOs aqueous dispersion turned black. Then, the mixture of dispersion was centrifuged at 2000 rpm for 30 min to remove unstabilized MWNTs. Next, the U/Ms were separated from the dispersion by removing the residual UMCNO with centrifugation (8000 rpm, 30 min) and water washing steps. Finally, the U/Ms were lyophilized. The obtained U/Ms were redispersed in water with sonication of 30 min. Figure 1c shows that the U/M aqueous dispersion is stable at room temperature without any precipitation upon storage for several weeks.

Similar to a dispersion of MWNTs with the assist of GO, it is reasonable to suppose that the π-conjugated multiple aromatic regions of the UMCNO could interact with the outer walls of MWNTs through the π-stacking interaction.[40,42,43] Therefore,

the U/Ms can be well-dispersed in water due to the presence of hydrophilic oxygen groups of UMCNOs. The ultraviolet−visible (UV-vis) and emission spectra were first used to characterize the combination of MWNTs and UMCNOs. As shown in Figure 2a, there is an evident absorption peak at 243 nm in the UV−vis absorption spectra of UMCNOs aqueous dispersion. It is ascribed to the $\pi \rightarrow \pi$ transition of aromatic C−C bonds of the UMCNOs. Comparison with the spectra of UMCNOs reveals that the absorption peak of U/Ms is centered at 264 nm, with an obvious redshift of 23 nm. Such shift is attributed to the π-stacking interaction between the multiple aromatic regions of UMCNOs and the sidewalls of MWNTs.[44−46] From the emission spectra (see Figure 2b), the UMCNOs is luminescent, showing a broad absorption band centered at ∼473 nm, as illustrated in the emission spectrum of UMCNOs. For pristine MWNTs, there is no emission at an excitation wavelength of 350 nm.[43] The U/Ms were formed by π-stacking interaction between the aromatic regions of UMCNOs and the sidewalls of MWNTs. As a result, the U/Ms also display an absorption band of luminescent at ∼473 nm. In addition, a new shoulder peak near ∼525 nm appears in the emission spectra of U/Ms. It may be attributed to the interfacial electron-transfer processes.[47−49] The photogenerated electrons from the aromatic regions of UMCNOs can transfer to attached MWNTs.[50] This is consistent with the measurement of UV−vis absorption.

UMCNOs possess oxygen-containing functional groups, such as carbonyl, carboxyl, and hydroxyl groups that existed at the edges and surfaces. When UMCNOs were attached to the surface of MWNTs by π-stacking interaction, the U/Ms exhibit good aqueous dispersibility. From the FTIR spectra of UMCNOs (see Figure 3a), the characteristic peaks for the stretch of carboxylic (−COOH) and hydroxyl (−OH) groups were observed at 1742 and 1224 cm^{-1}, respectively. The epoxy groups (C−O−C) exhibit the stretching vibrations at 1160 and 1051 cm^{-1}.[31,35] The U/Ms can be considered as hybrids of the MWNTs and UMCNOs. After UMCNOs were attached on the surface of MWNTs, the characteristic peaks for the stretching of the carboxylic groups (−COOH) and hydroxyl groups (C−OH) still appear at 1726 and 1251 cm^{-1} in the spectra of the U/Ms.[35,36]

To further study the dispersibility of U/Ms, we have measured the zeta potentials of the aqueous dispersions of the MWNTs, UMCNOs, and U/Ms at the same pH (4.6) by controlling the addition of 0.1 M hydrochloric acid. The zeta potential of the pristine MWNTs aqueous dispersion exhibited a positive value of ∼9.3 mV, and UMCNOs have negative zeta potentials of 35.1 mV because of the oxygen-containing groups on its surface.[51] With the presence of UMCNOs, the outer walls of MWNTs were coated with UMCNOs to form the U/M complex. The U/M water dispersion shows good stability. The U/Ms exhibit good aqueous dispersibility, with zeta potentials of 44.7 mV (negative). There is no sign for coagulation after more than one month. ASTM stipulates that colloids with zeta potentials of >40 mV (negative or positive) would have "good stability".[52,53] From the results of zeta potentials, the U/Ms exhibit better stability than the MWNTs and UMCNOs. It is implied that UMCNOs introduced into the surface of MWNTs would decrease the van der Waals attraction and conjugation among the individual MWNTs and UMCNOs itself.

The U/Ms can be considered as the hybrids of MWNTs and UMCNOs through conjugation with π-stacking interaction. X-ray diffraction (XRD) measurements were used to characterize the conjugation of MWNTs and UMCNOs (Figure 3b). The XRD patterns of pristine MWNTs revealed the presence of a peak at 2θ = 26.1°, corresponding to an interlayer spacing of 0.34 nm of the nanotube (d_{002}). The UMCNOs were obtained by oxidative unzipping of the MWNTs. Comparing the XRD patterns of MWNTs and UMCNOs, the (002) spacing shifted from 26.1° to 10.8°. This indicates that the MWNTs were unzipped and the compacted graphene layers have been loosened and exfoliated.[31,32,34] In addition, UMCNOs also have a minimal signal contributed by MWNTs (2θ = 22.2°), because of the residual structure of MWNTs, which was incompletely unraveled and exfoliated. Similar to GO, the UMCNOs exhibit some analogous characteristic after unzipping.[31,35] After oxidative unzipping, the oxygen functional groups were introduced into the UMCNOs.[33] The predominant peak at 10.8° of the UMCNOs, which corresponds to a *d*-spacing of 0.81 nm, is related to the oxygen functional groups in the intercalation of UMCNOs.[31,35] It can be attributed to the interlamellar water trapped between oxygen-containing functional groups on exfoliated GONR sheets in the UMCNOs.[54,55] In the XRD patterns of the U/Ms, there is no peak at ∼10.8°, because of the structure of the U/Ms.[34,44] With π-stacking interaction, the UMCNOs were attached onto the outer walls of MWNTs. The MWNTs then were inserted into the layer structure of UMCNOs. The U/Ms were not part of the layer structure, but rather a unique hybrid structure of one-dimensional (1D) nanotubes and two-dimensional (2D) UMCNOs.[31,33,43,56] In addition, the peaks at 22.2° and 26.1° also demonstrate the coexistence of MWNTs and UMCNOs.

Raman spectroscopy was also applied to characterize the U/Ms. As shown in Figure 4, the D and G bands of MWNTs at

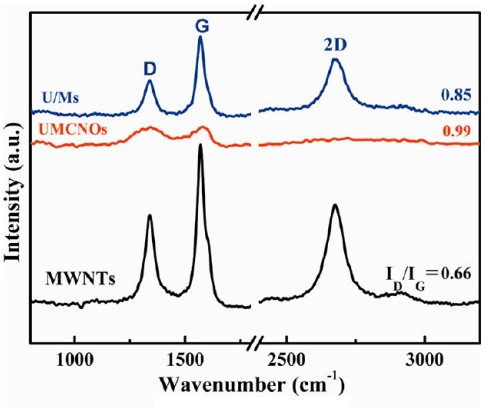

Figure 4. Raman spectroscopy of MWNTs, UMCNOs, and U/Ms.

1338 and 1569 cm^{-1} are attributed to the defects and disorder-induced modes and the in-plane E_{2g} zone-center mode, respectively.[57,58] The second prominent peak, the 2D band located at ∼2680 cm^{-1}, is originated from a double-resonance process.[59] After oxidation unzipping, the 2D band of pristine MWNTs disappeared in the UMCNO spectrum. It indicated a higher level of disorder of the GONR layers and defects increased during the oxidation unzipping process.[60] The D/G intensity ratio (I_D/I_G) is commonly used to indicate the average size of the C sp^2 domain. Compared to pristine MWNTs, the D/G intensity ratio for UMCNOs increases from 0.66 to 0.99, indicating the formation of some sp^3 carbon by oxidation.[33,61−64] However, for the U/Ms, the 2D band reappears

dx.doi.org/10.1021/am301623t | ACS Appl. Mater. Interfaces 2012, 4, 5956−5965

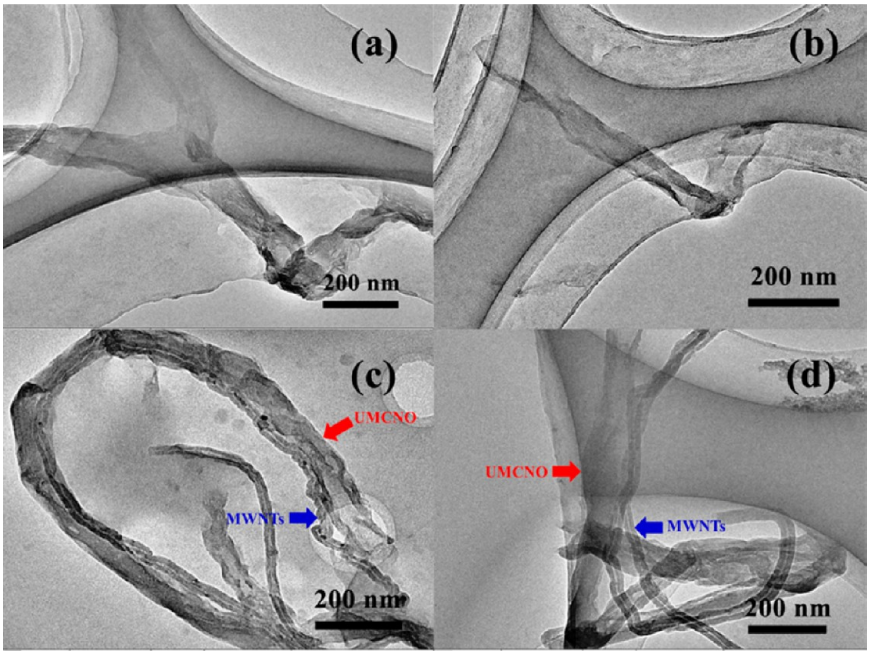

Figure 5. Selected TEM images of (a, b) UMCNOs and (c, d) U/Ms.

at ~2677 cm^{-1} after the introduction of MWNTs. In the meantime, the D/G intensity ratio for the U/Ms decreased to 0.85. This phenomenon can be attributed to the increase of the size of in-plane C sp^2 domains, possibly due to the introduction pristine MWNTs.[31,35,55]

TEM images offer direct information of the conjugation between UMCNOs and MWNTs. TEMs image of pristine MWNTs show a very smooth and clean surface. The tube structure of MWNTs can be clearly identified with inner and outer diameters along the length (see Figure S1 in the Supporting Information). UMCNOs were obtained by length-wise cutting and unraveling of MWNTs, using the method of step oxidation. As shown in Figure 5a, the walls of the MWNTs were cut off longitudinally and partly unfolded. Figure 5b shows that a folded, few-layer GONR was exfoliated from the walls of UMCNOs. After the MWNTs were adding into the UMCNOs aqueous dispersion, UMCNOs and MWNTs were combined together with the interaction of π-conjugated multiple aromatic regions of UMCNO and outer walls of MWNTs. Figures 5c and 5d show that the outer walls of MWNTs were attached with UMCNOs, which implied that the π-conjugated multiple aromatic regions of the UMCNO could interact with the outer walls of MWNTs through the $\pi-\pi$ stacking interaction.

Furthermore, TGA measurement was conducted to determine the content of the UMCNOs and MWNTs in U/Ms. As shown in Figure 6, it is observed that UMCNOs are thermally unstable and start to lose mass upon heating even below 100 °C, which is attributed to the volatilization of stored water in its π-stacked structure.[65] The major mass loss appears near 180 °C, which is attributed to the pyrolysis of oxygen-containing functional groups. Our calculation shows that U/Ms contain 61 wt % UMCNOs and 39 wt % MWNTs.

3.2. The U/Ms for Polymer Reinforcement. The U/Ms were obtained by dispersing MWNTs with the assist of UMCNOs. It can be well-dispersed in aqueous solution and exhibit good stability. With the synergistic effect of UMCNOs and MWNTs, the U/Ms can be used as ideal fillers for reinforcement of polymer. PVA was used as the model polymer

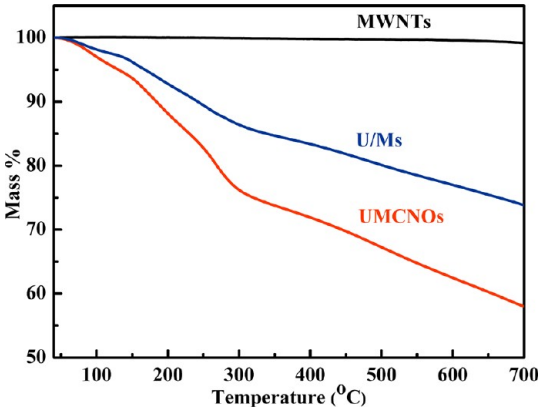

Figure 6. TGA curves of the MWNT, UMCNOs, and U/Ms.

to investigate the reinforcing efficiency of U/Ms. The U/M–PVA composite films with different amounts of U/Ms were fabricated by a simple solution-casting procedure. To maximize the advantages of fillers as effective reinforcements in high strength composites, the homogeneous dispersion of fillers in the polymer matrix is critical. The photographs of composite films with different loadings of U/Ms provide direct evidence for evaluating the quality of the composite films. In Figure 7, it was observed that all of the composite films are homogeneous with no noticeable aggregation. Optical microscope images were also used to evaluate the quality of the composite films from the smaller scale. As shown in Figure 8, the composite films with the low weight fraction (<0.7 wt %) are homogeneous and uniform, at least in micrometer-scale resolution. When the amount of U/Ms comes up to 1 wt %, many black shadows appear, which represent the agglomerations in the composite films.

The typical stress–strain response of the U/M–PVA composite films for 0.1, 0.3, 0.5, 0.7, and 1 wt % weight fractions of U/Ms additives are illustrated in Figure 9. Compared with pure PVA, the mechanical performance of

dx.doi.org/10.1021/am301623t | ACS Appl. Mater. Interfaces 2012, 4, 5956–5965

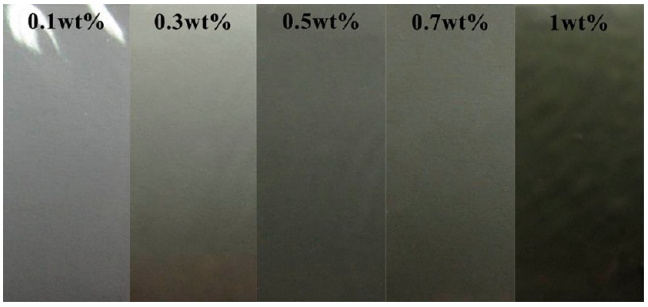

Figure 7. Photographs of U/M−PVA composite films with different amount of U/Ms (0.1, 0.3, 0.5, 0.7, and 1 wt %).

U/M−PVA composite films was improved. The yield of strength increased from 70.3 MPa to 98.7 MPa with only 0.1 wt % loading of U/Ms. The yield strength of the U/Ms/PVA composite film increased with the increase of U/Ms content. The maximum value of yield strength achieved 145.8 MPa with the incorporation of 0.7 wt % of U/Ms into a PVA matrix. However, the yield strength of a U/M−PVA composite film with 1 wt % U/Ms decreased to 107.3 MPa. It is attributed to the heavy agglomeration of U/Ms. We also conducted the SEM images of the fracture surface of the PVA composite films for studying the dispersion state of U/M−PVA composite films (see Figure S4 in the Supporting Information). As shown in Figure 10, it is shown that some bright dots and short lines were well-distributed in the U/M−PVA composite films with 0.1, 0.3, 0.5, and 0.7 wt %, and these were thought to be the U/Ms; no obvious agglomerations and cluster were found across the entire fracture surface. The images show that U/Ms were well-dispersed in the PVA matrix, and there was no indication of a large agglomeration or cluster of the U/Ms. For the U/M−PVA with 1 wt % U/Ms, there are obvious agglomerations in the PVA matrix (see Figure 10f). It is primary cause for the decrease of the yield strength of U/M−PVA composite film with 1 wt % U/Ms.

PVA is a semicrystalline polymer, and its mechanical properties are strongly dependent on the degree of crystallinity.[66,67] Polymer crystallinity can be determined with differential scanning calorimetry (DSC) by quantifying the heat associated with melting (fusion) of the polymer.[68] DSC was used to quantify the PVA crystalline fraction of U/M−PVA composites (see Figure 11). The degree of relative crystallinity (χ_c) was calculated as follows:

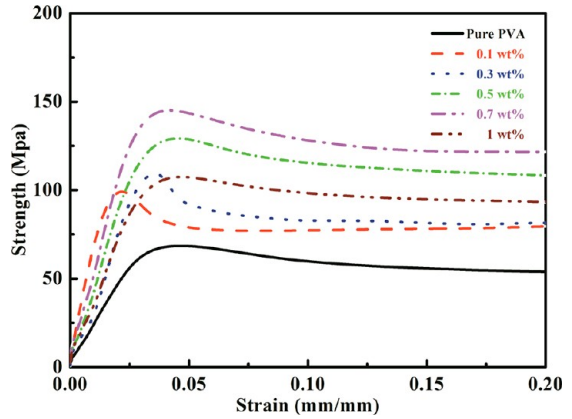

Figure 9. Typical stress−strain curves of the pure PVA and U/M−PVA composite films.

$$\chi_c = \frac{\Delta H_{m(T1\rightarrow T2)}}{\Delta H_0}$$

where $\Delta H_{m(T1\rightarrow T2)}$ is the measured melting enthalpy of the composite films and ΔH_0 is the enthalpy of fusion for 100% crystalline PVA (138.6 J/g).[69−71]

As shown in Table 1, the χ_c difference between the pure PVA and PVA-based composites is no more than 2.5%. The results imply that there is no obvious change of PVA crystallinity. Meanwhile, the degree of crystallinity values of PVA in the MWNT−PVA, UMCNO−PVA, and U/M−PVA composites were not changed on a large scale.

With the UMCNOs-assisted dispersion of MWNTs, it is expected that the mechanical properties of the U/M−PVA composite film would be better than that of MWNT−PVA and UMCNO−PVA composites. Thus, the tensile tests were also conducted for the MWNT−PVA and UMCNO−PVA composite films to characterize the reinforcement efficiency of U/Ms (see Table S1 in the Supporting Information). The filler loading was selected at 0.5 wt % for investigation, because the maximum yield strength of PVA composite films was achieved with incorporation of MWNTs at this loading (see Figure S3 in the Supporting Information). The stress−strain curves of MWNT−PVA, U/M−PVA, and UMCNO−PVA composite films are illustrated in Figure 12. Comparing with PVA, the yield strength of MWNT−PVA, UMCNO−PVA, and U/M−PVA composites at 0.5 wt % U/Ms were 79.8, 110.7, and

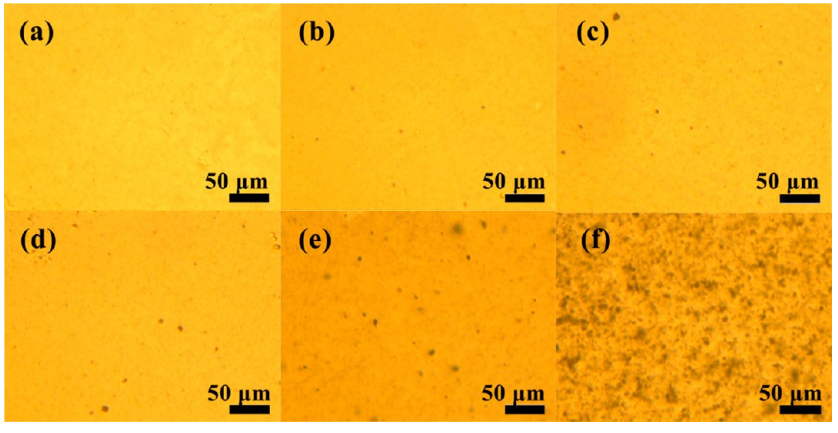

Figure 8. Optical images of U/M−PVA composite films: (a) pure PVA, (b) 0.1 wt %, (c) 0.3 wt %, (d) 0.5 wt %, (e) 0.7 wt %, and (f) 1 wt %.

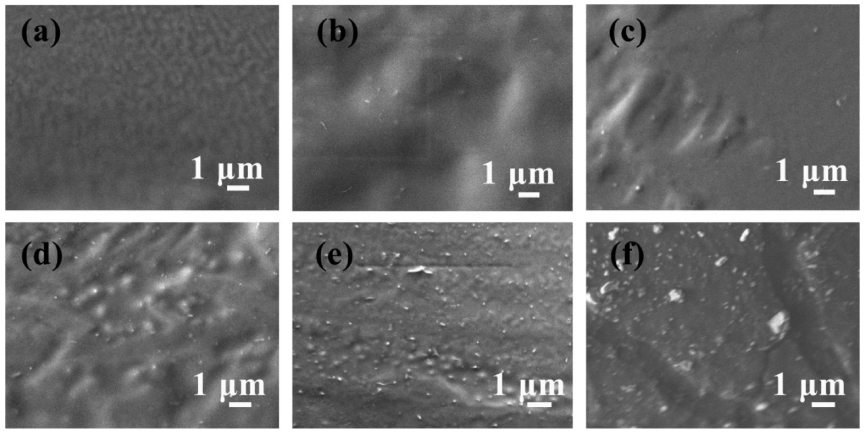

Figure 10. SEM images of fracture surfaces of (a) pure PVA and U/M−PVA composites films with (b) 0.1, (c) 0.3, (d) 0.5, (e) 0.7, and (f) 1 wt % U/Ms.

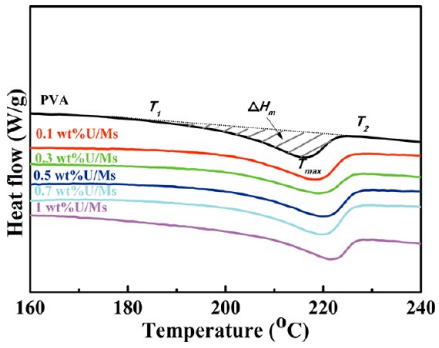

Figure 11. DSC curves of pure PVA and U/M−PVA composites films with different weight fractions.

Table 1. Crystallinity and Melting Enthalpy of Pure PVA and PVA-Based Composites

sample	ΔH_m (J/g)	X_c (%)
pure PVA	27.3	19.7
0.1 wt % U/Ms	26.5	19.1
0.3 wt % U/Ms	26.3	19.0
0.5 wt % U/Ms	27.8	20.1
0.7 wt % U/Ms	27.2	19.6
1 wt % U/Ms	27.6	20.0
0.5 wt % MWNTs	27.2	19.6
0.5 wt % UMCNOs	28.6	20.9

122.9 MPa, respectively, increased by ∼11.9%, ∼57.4%, and ∼74.8%, respectively. Obviously, the U/Ms show the highest reinforcement effect. This difference in mechanical properties is closely related with their dispersion and interaction toward the PVA matrix. Compared to pristine MWNTs, the UMCNOs have more available interface area (AIA) obtained from oxidative unzipping of MWNTs. Therefore, this strong interaction would result in higher reinforcement toward PVA than MWNTs. In the meantime, it is easy for UMCNOs to agglomerate in a polymer matrix with increasing loading (even at lower weight fractions), because of its 2D GNR-like structure.[34] SEM images of tensile fracture surfaces were also used to further characterize the dispersion and possible reinforcing mechanism. The tensile fracture surfaces of the PVA-based composites with the 5 wt % loading of fillers are illustrated in Figure 13. As shown in Figure 13a, the pulled-out MWNTs can be easily observed from the MWNTs/PVA

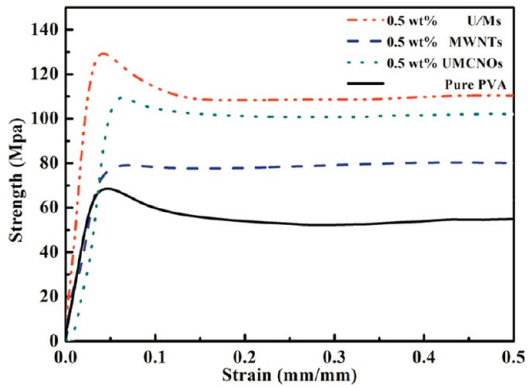

Figure 12. Typical stress−strain curves of the pure PVA, MWNT−PVA, UMCNO−PVA, and U/M−PVA composite films with 0.5 wt % weight fractions.

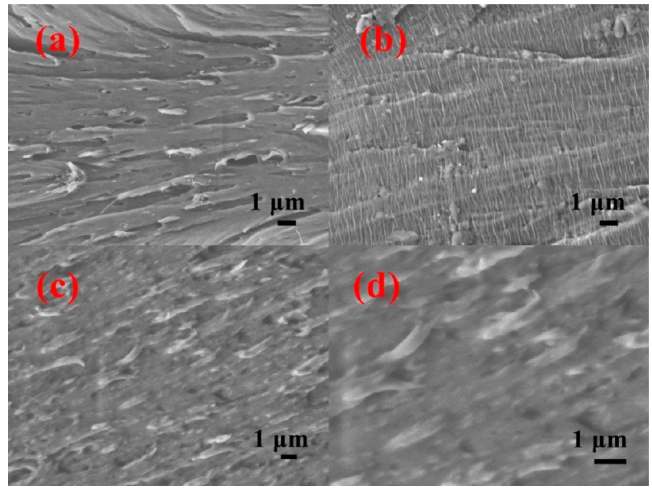

Figure 13. SEM images of fracture surface of composite films after tensile test: (a) MWNT−PVA composite films at the 0.5 wt % fillers loading, (b) UMCNO−PVA composite films at the 0.5 wt % fillers loading, (c) U/M−PVA composite films at the 0.5 wt % fillers loading, and (d) enlarged view of a partial area from panel (c).

composite films, which are denoted by red arrows. After oxidative unzipping, the individual UMCNO could hardly be observed in the PVA matrix. As a matter of fact, this is not unexpected from the previous characterizations of the GNR-

dx.doi.org/10.1021/am301623t | ACS Appl. Mater. Interfaces 2012, 4, 5956−5965

like structure of UMCNOs. However, there is an evident change in the feature of tensile fracture surfaces between the MWNT−PVA and U/M−PVA composite films (Figure 13c). The grooves, which were related to the broken or pulling-out U/Ms, are different from the MWNT−PVA composites after tensile tests (see Figure 13d). Obviously, they become more broaden after introduction of the MWNTs in the structure of the UMCNOs. It revealed that the UMCNOs were attached on the outer walls of the MWNTs, and a synergistic effect of UMCNOs and MWNTs in the PVA matrix was observed. In addition, with 0.5 wt % loading of the UMCNOs, some agglomerations of UMCNOs in PVA matrix were observed. These agglomerations deteriorated the dispersion of UMCNOs in PVA matrix and reduce the mechanical reinforcement.[34] The result is consistent with the decrease in yield strength and Young's modulus.

We also make a systematic study of mechanical properties for the UMCNO−PVA and U/M−PVA composites at series of loading fraction to illustrate the different enhancement behavior in mechanical properties. As shown in Figures 14 and 15, the

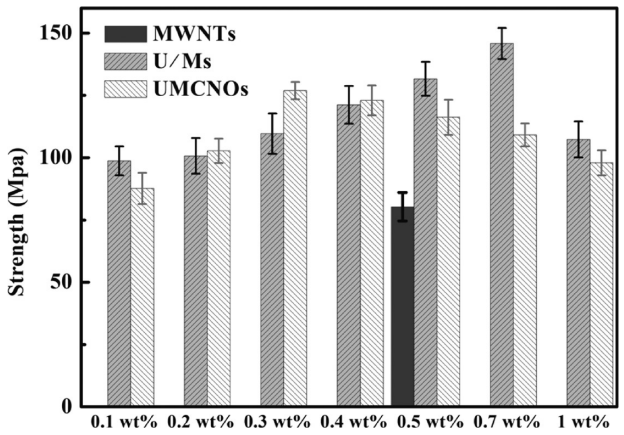

Figure 14. Yield strengths for the MWNT−PVA, UMCNO−PVA, and U/M−PVA composite films for various weight fractions of filler.

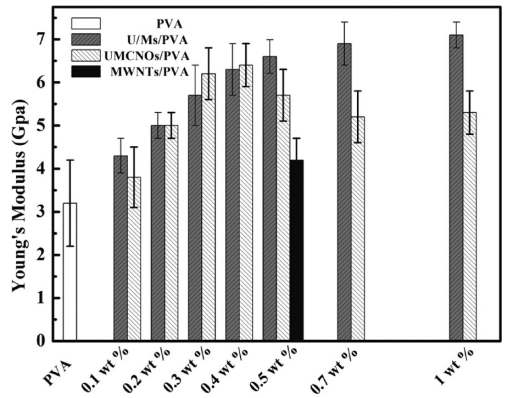

Figure 15. Young's modulus of the MWNT−PVA, UMCNO−PVA, and U/M−PVA composite films for various weight fractions of filler.

mechanical properties of PVA were both improved evidently with the addition of UMCNOs and U/Ms. With regard to the UMCNOs, the maximum yield strength and Young's modulus of the UMCNO−PVA composite film with 0.3 wt % weight fractions are 126.8 MPa and 6.2 GPa, respectively, increased by ∼80.3% and ∼93.6%, respectively, compared to PVA. With further increases in the UMCNOs loading (above 0.3 wt %), the yield strength and Young's modulus are gradually reduced. The results indicated that UMCNOs would be aggregated in the PVA matrix above a loading of 0.3 wt %. However, the U/M−PVA composite show quite different aggregated behaviors based on the analysis of the relationship between mechanical properties and the U/Ms loading. It is found that the yield strength and Young's modulus are increased as the U/Ms loading is increased from 0.1 wt % to 0.7 wt % and then reduced at 1 wt %, with a maximum yield strength and Young's modulus of ∼145.8 MPa and ∼6.9 GPa, respectively, which are higher than those for the UMCNO−PVA composite film (by ∼14.9% and ∼11.3%, respectively). The introduction of the MWNTs improved the dispersibility of the UMCNOs and reduced the agglomerations of the UMCNOs at a relatively high loading in a PVA matrix. The U/Ms exhibit high enhancement effect for mechanical reinforcement of PVA-based composites. The reinforcement effect of U/Ms was better than that of the individual MWNTs and UMCNOs, because of the synergistic effect of the combination of UMCNOs and MWNTs.

CONCLUSIONS

In summary, hybrids of unzipped multiwalled carbon nanotubes (UMCNOs) and multiwalled carbon nanotubes (MWNTs) (abbreviated as U/Ms) were prepared by adding pristine multiwalled nanotubes (MWNTs) into the UMCNOs aqueous dispersion, followed by sonication. With π-stacking interaction, the UMCNOs were attached onto outer walls of MWNTs. The U/Ms, which represent a hybrid structure of one-dimensional (1D) nanotubes and two-dimensional (2D) UMCNOs, can be well-dispersed in aqueous solution due to the hydrophilic surface of the UMCNOs. The U/Ms exhibit high enhancement effect for mechanical reinforcement of PVA-based composites. The results of tensile tests demonstrated that the reinforcement effect of U/Ms was better than the individual MWNTs and UMCNOs. In addition, the agglomeration phenomenon of reinforcing fillers in PVA matrix was obviously improved at a relatively high loading of the U/Ms. The yield strength and Young's modulus of U/M−PVA composites with a loading of 0.7 wt % of the U/Ms can reach ∼145.8 MPa and 6.9 GPa, which are increases of ∼107.4% and ∼122.5%, respectively. Therefore, the U/Ms show significantly potential as novel and effective reinforcement additives in polymer composites.

ASSOCIATED CONTENT

Supporting Information

This material is available free of charge via the Internet at http://pubs.acs.org.

AUTHOR INFORMATION

Corresponding Author

*Tel.: + 86-21-54743268. Fax: + 86-21-54747445. E-mail: zxshi@sjtu.edu.cn.

Notes

The authors declare no competing financial interest.

ACKNOWLEDGMENTS

We thank the National Nature Science Foundation of China (No. 50973062) for the support. In addition, we also acknowledge the staff of Instrumental Analysis Centre of Shanghai Jiao Tong University for the measurements.

REFERENCES

(1) Lin, Y.; Meziani, M. J.; Sun, Y.-P. *J. Mater. Chem.* **2007**, *17*, 1143−1148.
(2) Bokobza, L. *Polymer* **2007**, *48*, 4907−4920.
(3) Spitalsky, Z.; Tasis, D.; Papagelis, K.; Galiotis, C. *Prog. Polym. Sci.* **2010**, *35*, 357−401.
(4) Ajayan, P. M.; Stephan, O.; Colliex, C.; Trauth, D. *Science* **1994**, *265*, 1212−1214.
(5) Zhang, X.; Liu, T.; Sreekumar, T. V.; Kumar, S.; Moore, V. C.; Hauge, R. H.; Smalley, R. E. *Nano Lett.* **2003**, *3*, 1285−1288.
(6) Coleman, J. N.; Khan, U.; Gun'ko, Y. K. *Adv. Mater.* **2006**, *18*, 689−706.
(7) Coleman, J. N.; Khan, U.; Blau, W. J.; Gun'ko, Y. K. *Carbon* **2006**, *44*, 1624−1652.
(8) Andrews, R.; Weisenberger, M. C. *Curr. Opin. Solid State Mater. Sci.* **2004**, *8*, 31−37.
(9) Demczyk, B. G.; Wang, Y. M.; Cumings, J.; Hetman, M.; Han, W.; Zettl, A.; Ritchie, R. O. *Mater. Sci. Eng.: A* **2002**, *334*, 173−178.
(10) Chae, H. G.; Sreekumar, T. V.; Uchida, T.; Kumar, S. *Polymer* **2005**, *46*, 10925−10935.
(11) Jeon, J.-H.; Lim, J.-H.; Kim, K.-M. *Polymer* **2009**, *50*, 4488−4495.
(12) Zeng, H.; Gao, C.; Wang, Y.; Watts, P. C. P.; Kong, H.; Cui, X.; Yan, D. *Polymer* **2006**, *47*, 113−122.
(13) Wang, M.; Pramoda, K. P.; Goh, S. H. *Polymer* **2005**, *46*, 11510−11516.
(14) Lee, R.-S.; Chen, W.-H.; Lin, J.-H. *Polymer* **2011**, *52*, 2180−2188.
(15) Chen, G.-X.; Kim, H.-S.; Park, B. H.; Yoon, J.-S. *Polymer* **2006**, *47*, 4760−4767.
(16) Andrews, R.; Jacques, D.; Qian, D.; Rantell, T. *Acc. Chem. Res.* **2002**, *35*, 1008−1017.
(17) Wong, M.; Paramsothy, M.; Xu, X. J.; Ren, Y.; Li, S.; Liao, K. *Polymer* **2003**, *44*, 7757−7764.
(18) Lee, W. I.; Kim, S. H.; Park, J. M. *Carbon* **2009**, *47*, 2699−2703.
(19) Chou, T. W.; Thostenson, E. T. *Carbon* **2006**, *44*, 3022−3029.
(20) Yang, B. X.; Pramoda, K. P.; Xu, G. Q.; Goh, S. H. *Adv. Funct. Mater.* **2007**, *17*, 2062−2069.
(21) Coleman, J. N.; Cadek, M.; Ryan, K. P.; Nicolosi, V.; Bister, G.; Fonseca, A.; Nagy, J. B.; Szostak, K.; Beguin, F.; Blau, W. J. *Nano Lett.* **2004**, *4*, 353−356.
(22) Meng, H.; Sui, G. X.; Fang, P. F.; Yang, R. *Polymer* **2008**, *49*, 610−620.
(23) Hong, C.-Y.; You, Y.-Z.; Pan, C.-Y. *Polymer* **2006**, *47*, 4300−4309.
(24) Paiva, M. C.; Zhou, B.; Fernando, K. A. S.; Lin, Y.; Kennedy, J. M.; Sun, Y. P. *Carbon* **2004**, *42*, 2849−2854.
(25) Moniruzzaman, M.; Winey, K. I. *Macromolecules* **2006**, *39*, 5194−5205.
(26) Eitan, A.; Jiang, K.; Dukes, D.; Andrews, R.; Schadler, L. S. *Chem. Mater.* **2003**, *15*, 3198−3201.
(27) Hwang, G. L.; Shieh, Y. T.; Hwang, K. C. *Adv. Funct. Mater.* **2004**, *14*, 487−491.
(28) Yu, M.-F.; Lourie, O.; Dyer, M. J.; Moloni, K.; Kelly, T. F.; Ruoff, R. S. *Science* **2000**, *287*, 637−640.
(29) Sharma, R.; Strano, M. S. *Adv. Mater.* **2009**, *21*, 60−65.
(30) Wagner, H. D. *Chem. Phys. Lett.* **2002**, *361*, 57−61.
(31) Kosynkin, D. V.; Higginbotham, A. L.; Sinitskii, A.; Lomeda, J. R.; Dimiev, A.; Price, B. K.; Tour, J. M. *Nature* **2009**, *458*, 872−876.
(32) Zhang, Z.; Sun, Z.; Yao, J.; Kosynkin, D. V.; Tour, J. M. *J. Am. Chem. Soc.* **2009**, *131*, 13460−13463.
(33) Higginbotham, A. L.; Kosynkin, D. V.; Sinitskii, A.; Sun, Z.; Tour, J. M. *ACS Nano* **2010**, *4*, 2059−2069.
(34) Rafiee, M. A.; Lu, W.; Thomas, A. V.; Zandiatashbar, A.; Rafiee, J.; Tour, J. M.; Koratkar, N. A. *ACS Nano* **2010**, *4*, 7415−7420.
(35) Wang, Y.; Shi, Z.; Yin, J. *J. Phys. Chem. C* **2010**, *114*, 19621−19628.
(36) Fan, J.; Shi, Z.; Ge, Y.; Wang, Y.; Wang, J.; Yin, J. *Polymer* **2012**, *53*, 657−664.
(37) Wan, C.; Chen, B. *J. Mater. Chem.* **2012**, *22*, 3637−3646.
(38) Gong, L.; Kinloch, I. A.; Young, R. J.; Riaz, I.; Jalil, R.; Novoselov, K. S. *Adv. Mater.* **2010**, *22*, 2694−2697.
(39) Verdejo, R.; Bernal, M. M.; Romasanta, L. J.; Lopez-Manchado, M. A. *J. Mater. Chem.* **2011**, *21*, 3301−3310.
(40) Zhang, C.; Huang, S.; Tjiu, W. W.; Fan, W.; Liu, T. *J. Mater. Chem.* **2012**, *22*, 2427−2434.
(41) Li, Y.; Yang, T.; Yu, T.; Zheng, L.; Liao, K. *J. Mater. Chem.* **2011**, *21*, 10844−10851.
(42) Qian, Z.; Shaojun, Y.; Jing, Z.; Ling, Z.; Pingli, K.; Jinghong, L.; Jingwei, X.; Hua, Z.; Xi-Ming, S. *Nanotechnology* **2011**, *22*, 494010.
(43) Zhang, C.; Ren, L.; Wang, X.; Liu, T. *J. Phys. Chem. C* **2010**, *114*, 11435−11440.
(44) Guldi, D. M.; Rahman, G. M. A.; Jux, N.; Balbinot, D.; Hartnagel, U.; Tagmatarchis, N.; Prato, M. *J. Am. Chem. Soc.* **2005**, *127*, 9830−9838.
(45) Cheng, F.; Imin, P.; Maunders, C.; Botton, G.; Adronov, A. *Macromolecules* **2008**, *41*, 2304−2308.
(46) Ikeda, A.; Nobusawa, K.; Hamano, T.; Kikuchi, J.-i. *Org. Lett.* **2006**, *8*, 5489−5492.
(47) Lui, C. H.; Mak, K. F.; Shan, J.; Heinz, T. F. *Phys. Rev. Lett.* **2010**, *105*, 127404.
(48) Eda, G.; Lin, Y.-Y.; Mattevi, C.; Yamaguchi, H.; Chen, H.-A.; Chen, I. S.; Chen, C.-W.; Chhowalla, M. *Adv. Mater.* **2010**, *22*, 505−509.
(49) Gokus, T.; Nair, R. R.; Bonetti, A.; Böhmler, M.; Lombardo, A.; Novoselov, K. S.; Geim, A. K.; Ferrari, A. C.; Hartschuh, A. *ACS Nano* **2009**, *3*, 3963−3968.
(50) Williams, G.; Kamat, P. V. *Langmuir* **2009**, *25*, 13869−13873.
(51) Kim, Y. J.; Shin, T. S.; Choi, H. D.; Kwon, J. H.; Chung, Y.-C.; Yoon, H. G. *Carbon* **2005**, *43*, 23−30.
(52) Si, Y.; Samulski, E. T. *Nano Lett.* **2008**, *8*, 1679−1682.
(53) Zeta Potential of Colloids in Water and Waste Water, ASTM Standard D4187-82; *1985 Annual Book of ASTM Standards*; American Society for Testing and Materials: West Conshohocken, PA, 1985.
(54) Park, S.; An, J.; Jung, I.; Piner, R. D.; An, S. J.; Li, X.; Velamakanni, A.; Ruoff, R. S. *Nano Lett.* **2009**, *9*, 1593−1597.
(55) Pham, V. H.; Cuong, T. V.; Hur, S. H.; Oh, E.; Kim, E. J.; Shin, E. W.; Chung, J. S. *J. Mater. Chem.* **2011**, *21*, 3371−3377.
(56) Quintana, M.; Grzelczak, M.; Spyrou, K.; Calvaresi, M.; Bals, S.; Kooi, B.; Van Tendeloo, G.; Rudolf, P.; Zerbetto, F.; Prato, M. *J. Am. Chem. Soc.* **2012**, *134*, 13310−13315.
(57) Liao, S.-H.; Yen, C.-Y.; Hung, C.-H.; Weng, C.-C.; Tsai, M.-C.; Lin, Y.-F.; Ma, C.-C. M.; Pan, C.; Su, A. *J. Mater. Chem.* **2008**, *18*, 3993−4002.
(58) Yang, Y.; Xie, X.; Wu, J.; Yang, Z.; Wang, X.; Mai, Y.-W. *Macromol. Rapid Commun.* **2006**, *27*, 1695−1701.
(59) Su, C.-Y.; Xu, Y.; Zhang, W.; Zhao, J.; Tang, X.; Tsai, C.-H.; Li, L.-J. *Chem. Mater.* **2009**, *21*, 5674−5680.
(60) Guo, H.-L.; Wang, X.-F.; Qian, Q.-Y.; Wang, F.-B.; Xia, X.-H. *ACS Nano* **2009**, *3*, 2653−2659.
(61) Dresselhaus, M. S.; Jorio, A.; Hofmann, M.; Dresselhaus, G.; Saito, R. *Nano Lett.* **2010**, *10*, 751−758.
(62) Ferrari, A. C.; Meyer, J. C.; Scardaci, V.; Casiraghi, C.; Lazzeri, M.; Mauri, F.; Piscanec, S.; Jiang, D.; Novoselov, K. S.; Roth, S.; Geim, A. K. *Phys. Rev. Lett.* **2006**, *97*, 187401.
(63) Zhu, Y.; Murali, S.; Cai, W.; Li, X.; Suk, J. W.; Potts, J. R.; Ruoff, R. S. *Adv. Mater.* **2010**, *22*, 3906−3924.
(64) Kudin, K. N.; Ozbas, B.; Schniepp, H. C.; Prud'homme, R. K.; Aksay, I. A.; Car, R. *Nano Lett.* **2007**, *8*, 36−41.
(65) Jung, I.; Dikin, D.; Park, S.; Cai, W.; Mielke, S. L.; Ruoff, R. S. *J. Phys. Chem. C* **2008**, *112*, 20264−20268.
(66) Koski, A.; Yim, K.; Shivkumar, S. *Mater. Lett.* **2004**, *58*, 493−497.
(67) Cadek, M.; Coleman, J. N.; Barron, V.; Hedicke, K.; Blau, W. J. *Appl. Phys. Lett.* **2002**, *81*, 5123−5125.
(68) Kong, Y.; Hay, J. N. *Eur. Polym. J.* **2003**, *39*, 1721−1727.
(69) Peppas, N. A.; Merrill, E. W. *J. Appl. Polym. Sci.* **1976**, *20*, 1457−1465.

(70) Bhattacharyya, S.; Salvetat, J.-P.; Saboungi, M.-L. *Appl. Phys. Lett.* **2006**, *88*, 233119 (DOI: 10.1063/1.2209187).
(71) Asran, A. S.; Henning, S.; Michler, G. H. *Polymer* **2010**, *51*, 868−876.